Improved visualization of the subthalamic nucleus on synthetic MRI with optimized parameters: initial study

（視床下核の描出：最適化パラメータを用いた synthetic MRI による検討）

申請者　弘前大学大学院医学研究科
総合医療・健康科学領域 放射線診断学

氏名　　辰尾　小百合
指導教授　　掛田　伸吾

Abstract

Background: Synthetic MRI (SyMRI) enables to reformat various images by adjusting the MR parameters.

Purpose: The purpose was to investigate whether customization of the repetition time (TR), echo time (TE), and inversion time (TI) in SyMRI could improve the visualization of subthalamic nucleus (STN).

Material and Methods: We examined 5 healthy volunteers using both coronal SyMRI and quantitative susceptibility mapping (QSM), 7 patients with Parkinson's disease (PD) using coronal SyMRI, and 15 PD patients using coronal QSM. Two neuroradiologists reformatted SyMRI (optimized SyMRI) by adjusting TR, TE, and TI to achieve maximum tissue contrast between the STN and the adjacent brain parenchyma. The optimized MR parameters in the PD patients varied according to the individual. For regular SyMRI (T2WI and STIR), optimized SyMRI, and QSM, qualitative visualization scores of the STN (STN score) were recorded. The contrast-to-noise ratio (CNR) of the STN was also measured.

Results: For the STN scores in both groups, the optimized SyMRI were significantly higher than the regular SyMRI ($p < 0.05$), and no significant differences between optimized SyMRI and QSM. For the CNR of differentiation of the STN from the substantia nigra, the optimized SyMRI was higher than the regular SyMRI (volunteer; T2WI $p=0.10$ and STIR $p=0.26$, PD patient; T2WI $p=0.43$ and STIR $p=0.25$), but the optimized SyMRI was lower than the QSM (volunteer; $p=0.26$, PD patient; $p=0.03$).

Conclusions: On SyMRI, optimization of MR parameters (TR, TE, and TI) on an individual basis may be useful to increase the conspicuity of the STN.

Keywords:

synthetic MRI; magnetic resonance imaging; Parkinson's disease; subthalamic nucleus; substantia nigra; quantitative susceptibility mapping

Introduction

The subthalamic nucleus (STN) is a surgical target of deep brain stimulation (DBS), which is an accepted surgical treatment for advanced Parkinson disease (PD) (1,2). Because the success of DBS is mostly dependent on accurate positioning of the leads at the optimal target point, the STN (3,4). Thus, direct visualization of the STN by MRI is challenging.

The STN is a lens-shaped structure that is smaller than 1.5 cm and biconvex in the coronal plane. It is located in the caudal subthalamic region, and bordered superiorly by the zona incerta (ZI) and lenticular fasciculus and inferiorly by the substantia nigra (SN) (5,6). In the coronal MRI plane perpendicular to the anterior commissure–posterior commissure line (AC-PC line), and at the level of internal auditory canal, the STN and SN are found within the same plane, with the STN located cranial and laterally adjacent to the SN (Fig. 1). More recently, 7T MRI has been approved for clinical imaging. Although 7T MRI has been utilized for superior visualization (7,8), 7T MRI is limited by its high cost and low availability at the moment.

In most reported cases, the T2-weighted sequence was used for visualizing the STN (9,10). On T2-weighted imaging (T2WI), the STN shows a low-intensity signal in comparison to the surrounding white matter because of the susceptibility effect from the iron within the STN (although the STN is grey matter). More recently, Liu et al. reported that a novel MRI technique at 3T, quantitative susceptibility mapping (QSM), significantly improved visualization of the STN in comparison to the current standard MRI sequences (T2WI, T2*WI, or susceptibility-weighted imaging:

SWI) (11). The QSM technique is insensitive to the geometry of veins and dipolar artefacts; both of which affect the distribution of measured phase values. On QSM, the STN can appear hyperintense due to iron deposition within the STN (11). However, as a limitation of the QSM technique, QSM images are affected by blooming artifacts, which depend on susceptibility, echo time, and field strength (11,12). Furthermore, QSM images are obtained with a 3D gradient echo (GRE) sequence, which is sensitive to patients' motion during MRI acquisitions, so its application in patients with obvious tremor may be limited. Clinically, postprocessing for QSM requires additional tools to perform complex calculations, and QSM images cannot be acquired in-line during clinical MRI examinations. Thus, various MRI sequences or techniques have been used in attempts to depict the STN.

On conventional MRI, image contrast is mainly influenced by two parameters, the repetition time (TR) and the echo time (TE), which are determined in advance. Synthetic MRI (SyMRI) was recently introduced to enable the accurate quantification of MR images (13,14), which makes it possible to reformat SyMRI in various ways by adjusting MR parameters such as the TR, TE, and inversion time (TI) (15,16). A previous study showed that SyMRI with the optimization of the TR and TE for shoulder MR arthrography enabled the optimization of soft-tissue contrast (17). However, no study to date has addressed optimization for the identification of the STN using SyMRI. We hypothesized that optimized SyMRI can be reformatted by adjusting the TR, TE, and TI to achieve maximum tissue contrast between the STN and the adjacent brain parenchyma. The purpose of this pilot study was to investigate whether customization of the TR, TE, and TI on SyMRI can improve the

visualization of the STN.

Materials and Methods

Subjects

This study was approved by our institutional review board. This study included 5 healthy volunteers (Table 1). All healthy volunteers gave their written informed consent before MR imaging, which included SyMRI and QSM.

From the MRI database of patients who underwent SyMRI or QSM, we retrospectively selected 7 PD patients who had been examined by coronal SyMRI, and 15 patients who had been examined by coronal QSM. Thus, the study included a total of 22 PD patients who fulfilled the UK Parkinson's Disease Society Brain Bank criteria for the diagnosis of idiopathic PD; PD patients were on anti-parkinsonian medication at the time of testing. In the case of the PD patients, our institutional review board approved this retrospective assessment and waived the need for informed consent.

Magnetic Resonance Imaging (MRI)

SyMRI was performed using a 3T system (3T Magnetom Vida; Siemens) with a 20-channel head coil. Details of the synthetic MR sequence acquisition have been described elsewhere (13,15,18,19). SyMRI was implemented as a saturation recovery turbo spin-echo (TSE) sequence with a saturation pulse flip angle of 120°, a multiecho readout including phase and magnitude data, with 4 repetitions. The section acquisition order was altered for each repetition, resulting in 4 different effective

saturation delays (150, 580, 2000, and 4130 ms) for each section. The imaging parameters were as follows: number of excitations, 1; section thickness, 2.2 mm; matrix, 320 × 240; field of view, 24 × 24 cm; and imaging time, 12 minutes 14 seconds. A parallel imaging method (generalized autocalibrating partially parallel acquisitions) was used with a reduction factor of 2. The resulting data formed a matrix of 8 complex images per section at different saturation delays and TEs. SyMRI was obtained from the quantitative Qmap data, with operator-specified TR, TE, and TI values, using the SyMRI version 7.2 RC2 software package (SyntheticMR AB, Linkoping, Sweden). For the purposes of our study, standardized TR, TE, and TI values were used to produce comparable synthetic T2WI (Sy-T2WI) and short inversion time inversion-recovery (STIR) sequences (Sy-STIR) based upon comparison with clinical sequences performed at our institution (Table 2). SyMRI data were obtained using the TSE sequence, and signal intensities on SyMRI were calculated based on the fitting algorithm (15). Therefore, the relationship between image contrast and the sequence parameters of SyMRI do not correlate with that of conventional MRI. In the present study, regular SyMRI (Sy-STIR) was performed using standard manufacturer-recommended sequence parameters, which differed from the sequence parameters of conventional STIR described in previous reports (6,20). We thus confirmed that the image contrast of Sy-STIR was similar to that with conventional STIR. Furthermore, Sy-STIR with a TI of 300 ms had the best image contrast for fat-suppressed imaging.

Technologically, in our institution, QSM was not available using the 3-Tesla MR scanner (3T Magnetom Vida; Siemens). Therefore, QSM studies were performed on a 3T MRI system (Signa

EXCITE 3T; GE Healthcare, Chicago, IL, USA) using a dedicated eight-channel phased-array coil (USA Instruments Aurora, OH, USA). QSM was reconstructed from data (magnitude and phase images) obtained using 3D multi-echo spoiled GRE imaging using the Cornell QSM software package (21,22), which included various algorithms (unwrapping algorithm, projection onto dipole field [PDF] algorithm, a standard FSL-Brain Extraction Tool [BET] algorithm). The local magnetic field was calculated from a field map derived from MR phase images. Unwrapping of the combined phase data was performed on the field estimated from multiple echo complex data using the image quality-guided unwrapping algorithm, as described and recommended in a previous report (23,24). A frequency or field map was also generated from all echoes according to the methods described previously (23). For the background field removal technique, the PDF algorithm was used (25). Brain masking (skull stripping) for the QSM was performed using a standard FSL-BET algorithm (26,27). Finally, the QSM was reconstructed using GRE images (magnitude and wrapped phase images) by a morphology-enabled dipole inversion (MEDI) technique (23). The MEDI technique, for the generation of the morphology mask, inverts the estimated local magnetic field to generate a magnetic susceptibility distribution that constitutes the magnitude image. Such post-processing cannot be performed in an in-line manner. The QSM images were available approximately 10 min after data had been transferred to a workstation.

Optimized SyMRI

By visual assessment of two neuroradiologists (H.S., S.K.; 17 and 24 years of radiology experience,

respectively), to determine the point with maximum contrast in SyMRI, differences in SI between the STN and adjacent brain parenchyma were simulated by varying TR, TE, and TI within ranges of 4387-11833ms, 18-76ms, and 0-5936ms, respectively (Table 2). The optimization with SyMRI were performed based on a previously described qualitative visualization score of the STN (STN-score) (11): Score 0, the STN was not visible; Score 1, the STN-SN complex was poorly visible with fuzzy borders; Score 2, only the superior border of the STN and not the border with SN was visible; and Score 3, the STN was well defined and clearly differentiable from its superior neighbor, presumably the zona incerta (ZI), and its inferior neighbor, the SN (Fig. 1 and 2).

Qualitative Image Assessment

Optimized SyMRI, as well as regular SyMRI (T2WI and STIR) and QSM, were independently assessed by two experienced neuroradiologists (F.T., S.I.; 19 and 15 years of radiology experience, respectively) using the STN-score (11). Coronal brain sections of each subject obtained with all imaging methods were presented to each of the neuroradiologists simultaneously. After independent interpretations were performed, the differences in assessments between the two radiologists were resolved by consensus.

Quantitative Image Assessment

All image data were transferred to a workstation (Ziostation-2; Ziosoft/AMIN, Tokyo, Japan), and all measurements were performed on same monitor (RadiForce MX242W; EIZO). According to previously published methods (11), a radiologist (S.T., 3 years of experience) measured the

contrast-to-noise ratio (CNR) of the STN on all images. For each subject, bilateral regions of interest were manually drawn on the single section recorded from the previous qualitative assessment on the image with the highest visualization score (Fig. 1). After delineating the STN, a 2-mm band tracing the superior border of the STN and a 1-mm band tracing the inferior border of the STN were drawn to calculate the difference in intensity between the STN and its superior neighbor, presumably the ZI, and its inferior neighbor, the SN. These regions of interest (ROIs) were then propagated onto the complete set of images (SyMRI and QSM). The contrast on each image was calculated as the absolute difference between the mean value in the STN and the mean value in the surrounding bands. Noise was measured by calculating the standard deviation of the signal intensity in the thalamus due to its relatively uniform signal intensity (11).

Statistical Analysis

Differences between the PD patients evaluated by SyMRI and the PD patients evaluated by QSM were compared using Fisher's exact test for sex and the Mann–Whitney U test for age, disease onset, disease duration, and disease severity (Hoehn and Yahr stage). In the healthy volunteers, the Friedman test was used to assess the variation regarding the STN score and CNR measurements across the 4 MRI sequences (Sy-T2WI, Sy-STIR, optimized SyMRI, and QSM). Then pair-wise comparisons among the 4 MRI sequences were performed using Wilcoxon signed rank tests. In the PD patients, the Kruskal-Wallis test was used to assess the variation in STN score and CNR measurements across the 4

MRI sequences. Then pair-wise comparisons among the 4 MRI sequences were performed using the Steel-Dwass test. P values of <0.05 were considered to indicate statistical significance.

Interobserver agreement for the qualitative assessment was calculated as a weighted κ value. The strength of agreement was considered fair for κ values of 0.21–0.40, moderate for κ values of 0.41–0.60, good for κ values of 0.61–0.80, and excellent for κ values of ≥0.81. All statistical analyses were performed using the R software program.

Results

Optimized SyMRI

For each subject, two neuroradiologists optimized the TR, TE, and TI values on SyMRI to achieve ideal contrast. The optimized MR parameters are shown in Table 2. In all healthy volunteers, the neuroradiologists could achieve the maximum contrast between the STN and the adjacent brain parenchyma using one set of values (TR=5000 msec, TE=40 msec) without an inversion recovery method, although the MR parameters varied slightly from subject to subject (Table 2). In contrast to the healthy volunteers, the optimized TR, TE, and TI values were found to vary among PD patients (Table 2).

Qualitative Image Assessment

In all healthy volunteers and PD patients, the STN appeared hypointense and lenticular on region-specific SyMRI (Fig. 2). The STN scores for optimized SyMRI, Sy-T2WI, Sy-STIR, and QSM

are shown in Table 3. In healthy volunteers and PD patients, the STN scores on optimized SyMRI were significantly higher than those on Sy-T2WI and Sy-STIR (p <0.05). The median (interquartile range) STN scores for optimized SyMRI in our healthy volunteers and PD patients were 3 (3-3) and 3 (3-3), respectively, which was comparable to those for QSM: 3 (3-3) and 3 (2-3).

For optimized SyMRI and QSM, the κ values for interobserver variability between the two radiologists were 0.4324 and 0.5181, indicating moderate interobserver agreement.

Quantitative Image Assessment

For the STN-ZI, optimized SyMRI showed a higher median CNR in comparison to Sy-STIR. For the STN-SN, the CNR on optimized SyMRI was higher than that on regular SyMRI (Sy-T2WI and Sy-STIR), whereas there were no significant differences between them (Table 4). In both healthy volunteers and PD patients, for each category, optimized SyMRI showed a lower CNR in comparison QSM; there were significant differences between the two modalities (Table 4).

Discussion

The recently introduced SyMRI technology allows post-acquisition modulation of TR and TE with just one acquisition (15,16). In this study, neuroradiologists optimized the TR, TE, and TI values on SyMRI to achieve ideal contrast between the STN and adjacent brain parenchyma. The results demonstrated that optimized SyMRI provided superior image quality for the depiction of the STN in comparison to regular SyMRI.

In previous studies of SyMRI (28-31), once an imaging pulse sequence was optimized, sequence parameters were saved and subsequently used to acquire data from all subjects. In our healthy volunteers, the fixed protocol (TR=5000 msec, TE=40 msec) could generate clear contrast between the low signal from the STN and the high signal from the surrounding white matter. This method may be defined as region-specific SyMRI. In contrast to healthy volunteers, the optimal TR, TE, and TI values for maximal contrast of the STN were found to vary among our PD patients. Thus, the optimized MR parameters in PD patients, which varied according to the individual, may be defined as patient-specific MR parameters. Importantly, for both the qualitative and quantitative assessments, it was confirmed that SyMRI with patient-specific MR parameters was superior to regular SyMRI for STN conspicuity.

In elderly patients with PD, an optimized TI was found to produce an improvement in regional contrast between the STN and SN. The current result may be supported by the previous finding that the STIR method, an inversion-recovery pulse sequence, was suitable for delineating the STN in contrast to surrounding white matter (20). Kitajima et al. also showed that the combined reading of both T2WI and STIR at 3T improved the identification of the STN (6). As a major advantage, STIR shows strong contrast between the gray and white matter (32,33). Thus, the inversion-recovery pulse sequences may generate clear contrast between the STN and the adjacent brain parenchyma.

In this study, the value of patient-specific MR parameters varied in individual PD patients. This may be due to pathology-related changes of the SN in PD patients. Increased nigral iron content in

PD patients is a prominent pathophysiological feature involved in selective dopaminergic neurodegeneration of the SN (34,35). A previous study reported that susceptibility due to increased nigral iron content in PD reflected the signal intensity of the SN (36,37), which may obscure the boundary between the STN and SN. Moreover, another previous study found that the susceptibility effect of the SN in PD patients was correlated with disease severity according to the Hoehn and Yahr stage (38). This suggests that the signal intensity of the SN in PD patients may ordinarily vary according to the individual.

In our quantitative image assessment optimized SyMRI showed lower CNR values in comparison to QSM. However, we believe that for detecting targets for DBS, it is important to identify the STN using a qualitative image assessment on an individual basis**.** The STN scores of optimized SyMRI in healthy volunteers and PD patients were comparable to the STN scores of QSM. On QSM, the paramagnetic field effects can be quantified. Therefore, for the depiction of STN, the QSM is sensitive molecular environment regarding T2* weighted values (11,37). On the other hand, the image contrast on SyMRI depends on relaxation-based methods; the signal comes from the precession of water protons after radio-frequency (RF) excitation, and then gradually decays at a relaxation rate that is determined by the local molecular environment. In some PD patients, we found that the boundary between the STN and the SN on QSM was indistinct because both the STN and the SN showed hyperintensity (Fig. 3). On the other hand, on optimized SyMRI, the STN appeared hypointense in comparison to the adjacent brain parenchyma. Therefore, the SyMRI and QSM provide different

information for the assessment of the depiction of the STN, and it is important to note that this represents complementary information. For the planning of DBS, both techniques are also complementary and more useful compared to conventional MRI. Because SyMRI (T1WI, T2WI or FLAIR) is derived from an identical dataset (from one single acquisition), in contrast to conventional imaging, there no misregistration artifacts were found when fusion images were created using SyMRI. This advantage may improve neurosurgical targeting and the planning of DBS. For planning of DBS with QSM, precise depiction of the internal structures of the globus pallidus, as well as STN, has been also useful for targeting of the globus pallidus internus (39,40). For targeting these anatomical structures, more recent investigators used a whole brain image with skull, which created by combining the magnitude image and QSM image (39) .

The present study was associated with several limitations. The number of patients in this study was small and, consequently, the results suggesting that the depiction of the STN was improved on SyMRI will need to be validated in a larger independent sample of patients before any general conclusions can be drawn regarding improvements in DBS and the evaluation of the brain in PD patients. Although the regular SyMRI (Sy-T2WI and Sy-STIR) was performed using standard manufacturer-recommended pulse sequences and settings, more optimal sequence protocols for the evaluation of STN may exist. Moreover, in this study, the MR parameters on SyMRI were optimized by a qualitative assessment by neuroradiologists. Thus, the images obtained from these protocols may still be suboptimal at the individual patient level. This study used 2D data. We expect future studies to

evaluate the feasibility of SyMRI using 3D data acquisition (41,42).

In conclusion, the STN contrast was maximized by adjusting the TR, TE, and TI values. In the present study, the optimized MR parameters that obtained maximal STN contrast were found to vary among the PD patients, indicating that patient-specific MR parameters should be optimized for the depiction of the STN. This concept of achieving maximal tissue contrast can be extended to other brain regions as well.

References

1. Kumar R, Lozano AM, Kim YJ, et al. Double-blind evaluation of subthalamic nucleus deep brain stimulation in advanced Parkinson's disease. Neurology 1998;51:850-855. DOI: 10.1212/wnl.51.3.850.

2. Limousin P, Krack P, Pollak P, et al. Electrical stimulation of the subthalamic nucleus in advanced Parkinson's disease. N Engl J Med 1998;339:1105-1111. DOI: 10.1056/NEJM199810153391603.

3. Paek SH, Yun JY, Song SW, et al. The clinical impact of precise electrode positioning in STN DBS on three-year outcomes. J Neurol Sci 2013;327:25-31. DOI: 10.1016/j.jns.2013.01.037.

4. Okun MS, Tagliati M, Pourfar M, et al. Management of referred deep brain stimulation failures: a retrospective analysis from 2 movement disorders centers. Arch Neurol 2005;62:1250-1255. DOI: 10.1001/archneur.62.8.noc40425.

5. Massey L, Miranda M, Zrinzo L, et al. High resolution MR anatomy of the subthalamic nucleus: imaging at 9.4 T with histological validation. Neuroimage 2012;59:2035-2044.

6. Blinded for anonymity

7. Abosch A, Yacoub E, Ugurbil K, et al. An assessment of current brain targets for deep brain stimulation surgery with susceptibility-weighted imaging at 7 tesla. Neurosurgery 2010;67:1745-1756.

8. Cho Z-H, Min H-K, Oh S-H, et al. Direct visualization of deep brain stimulation targets in Parkinson disease with the use of 7-tesla magnetic resonance imaging. J Neurosurg 2010;113:639-647.

9. Starr PA, Christine CW, Theodosopoulos PV, et al. Implantation of deep brain stimulators into subthalmic nucleus: technical approach and magnetic imaging—verified electrode locations. J Neurosurg 2002;97:370-387.

10. Zonenshayn M, Rezai AR, Mogilner AY, et al. Comparison of anatomic and neurophysiological methods for subthalamic nucleus targeting. Neurosurgery 2000;47:282-292; discussion 292-284. DOI: 10.1097/00006123-200008000-00005.

11. Liu T, Eskreis-Winkler S, Schweitzer AD, et al. Improved subthalamic nucleus depiction with quantitative susceptibility mapping. Radiology 2013;269:216-223. DOI: 10.1148/radiol.13121991.

12. Li J, Chang S, Liu T, et al. Reducing the object orientation dependence of susceptibility effects in gradient echo MRI through quantitative susceptibility mapping. Magn Reson Med 2012;68:1563-1569.

13. Riederer SJ, Suddarth SA, Bobman SA, et al. Automated MR image synthesis: feasibility studies. Radiology 1984;153:203-206. DOI: 10.1148/radiology.153.1.6089265.

14. Warntjes MJ, Kihlberg J, Engvall J. Rapid T1 quantification based on 3D phase sensitive inversion recovery. BMC Med Imaging 2010;10:19. DOI: 10.1186/1471-2342-10-19.

15. Warntjes JB, Leinhard OD, West J, et al. Rapid magnetic resonance quantification on the brain: Optimization for clinical usage. Magn Reson Med 2008;60:320-329. DOI: 10.1002/mrm.21635.

16. Meara SJ, Barker GJ. Evolution of the longitudinal magnetization for pulse sequences using a fast spin-echo readout: Application to fluid-attenuated inversion-recovery and double inversion-recovery sequences. Magn Reson Med 2005;54:241-245.

17. Lee SH, Lee YH, Hahn S, et al. Optimization of T2-weighted imaging for shoulder magnetic resonance arthrography by synthetic magnetic resonance imaging. Acta Radiol 2018;59:959-965. DOI: 10.1177/0284185117740761.

18. Warntjes JB, Engström M, Tisell A, et al. Brain characterization using normalized quantitative magnetic resonance imaging. PloS one 2013;8:e70864.

19. Warntjes JB, Dahlqvist O, Lundberg P. Novel method for rapid, simultaneous T1, T2*, and proton density quantification. Magn Reson Med 2007;57:528-537. DOI: 10.1002/mrm.21165.

20. Taoka T, Hirabayashi H, Nakagawa H, et al. “Sukeroku sign” and “dent internal-capsule sign”—identification guide for targeting the subthalamic nucleus for placement of deep brain stimulation electrodes. Neuroradiology 2009;51:11.

21. de Rochefort L, Liu T, Kressler B, et al. Quantitative susceptibility map reconstruction from MR phase data using bayesian regularization: validation and application to brain imaging. Magn Reson Med 2010;63:194-206.

22. Schweser F, Robinson SD, de Rochefort L, et al. An illustrated comparison of processing methods for phase MRI and QSM: removal of background field contributions from sources outside the region of interest. NMR Biomed 2017;30:e3604. DOI: 10.1002/nbm.3604.

23. Liu T, Surapaneni K, Lou M, et al. Cerebral microbleeds: burden assessment by using quantitative susceptibility mapping. Radiology 2012;262:269-278.

24. Langkammer C, Liu T, Khalil M, et al. Quantitative susceptibility mapping in multiple sclerosis. Radiology 2013;267:551-559. DOI: 10.1148/radiol.12120707.

25. Liu T, Khalidov I, de Rochefort L, et al. A novel background field removal method for MRI using projection onto dipole fields. NMR Biomed 2011;24:1129-1136.

26. Liu T, Liu J, de Rochefort L, et al. Morphology enabled dipole inversion (MEDI) from a single-angle acquisition: comparison with COSMOS in human brain imaging. Magn Reson Med 2011;66:777-783. DOI: 10.1002/mrm.22816.

27. Smith SM. Fast robust automated brain extraction. Hum Brain Mapp 2002;17:143-155. DOI: 10.1002/hbm.10062.

28. West H, Leach JL, Jones BV, et al. Clinical validation of synthetic brain MRI in children: initial experience. Neuroradiology 2017;59:43-50. DOI: 10.1007/s00234-016-1765-z.

29. Krauss W, Gunnarsson M, Nilsson M, et al. Conventional and synthetic MRI in multiple sclerosis: a comparative study. Eur Radiol 2018;28:1692-1700. DOI: 10.1007/s00330-017-5100-9.

30. Granberg T, Uppman M, Hashim F, et al. Clinical Feasibility of Synthetic MRI in Multiple Sclerosis: A Diagnostic and Volumetric Validation Study. AJNR Am J Neuroradiol 2016;37:1023-1029. DOI: 10.3174/ajnr.A4665.

31. Ryu KH, Choi DS, Baek HJ, et al. Clinical feasibility of 1-min ultrafast brain MRI compared with routine brain MRI using synthetic MRI: a single center pilot study. J Neurol 2019;266:431-439.

32. Oikawa H, Sasaki M, Tamakawa Y, et al. The substantia nigra in Parkinson disease: proton density-weighted spin-echo and fast short inversion time inversion-recovery MR findings. AJNR Am J Neuroradiol 2002;23:1747-1756.

33. Saeki N, Kansaku K, Higuchi Y, et al. Demonstration of the postcommissural fibres of the fornix in short-inversion time inversion-recovery imaging on a high-field system. Neuroradiology 2001;43:547-550. DOI: 10.1007/s002340100549.

34. Dexter DT, Carayon A, Javoy-Agid F, et al. Alterations in the levels of iron, ferritin and other trace metals in Parkinson's disease and other neurodegenerative diseases affecting the basal ganglia. Brain 1991;114 (Pt 4):1953-1975. DOI: 10.1093/brain/114.4.1953.

35. Graham JM, Paley MN, Grünewald RA, et al. Brain iron deposition in Parkinson's disease imaged using the PRIME magnetic resonance sequence. Brain 2000;123:2423-2431.

36. Blinded for anonymity

37. Blinded for anonymity

38. Jin L, Wang J, Zhao L, et al. Decreased serum ceruloplasmin levels characteristically aggravate nigral iron deposition in Parkinson's disease. Brain 2011;134:50-58. DOI: 10.1093/brain/awq319.

39. Wei H, Zhang C, Wang T, et al. Precise targeting of the globus pallidus internus with quantitative susceptibility mapping for deep brain stimulation surgery. J Neurosurg 2019;133:1-7. DOI: 10.3171/2019.7.JNS191254.

40. Blinded for anonymity

41. Fujita S, Hagiwara A, Hori M, et al. 3D quantitative synthetic MRI-derived cortical thickness and subcortical brain volumes: Scan-rescan repeatability and comparison with conventional T1 -weighted images. J Magn Reson Imaging 2019;50:1834-1842. DOI: 10.1002/jmri.26744.

42. Fujita S, Hagiwara A, Otsuka Y, et al. Deep learning approach for generating MRA images from 3D quantitative synthetic MRI without additional scans. Invest Radiol 2020;55:249-256.

FIGURE 1

(a)

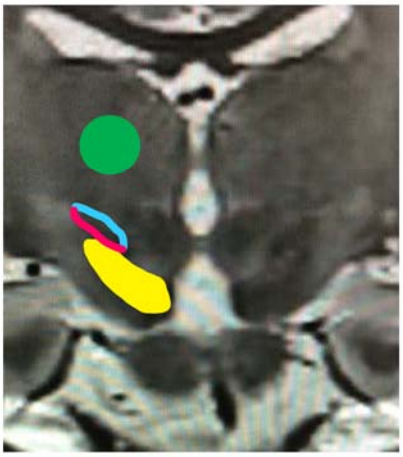

(b)

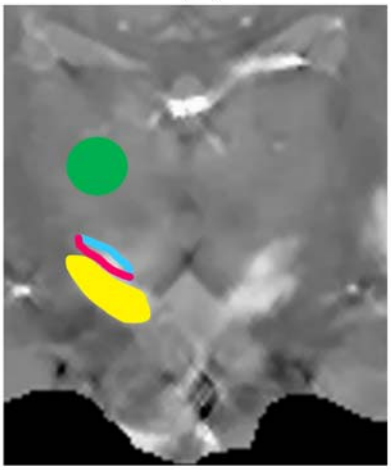

FIGURE 2

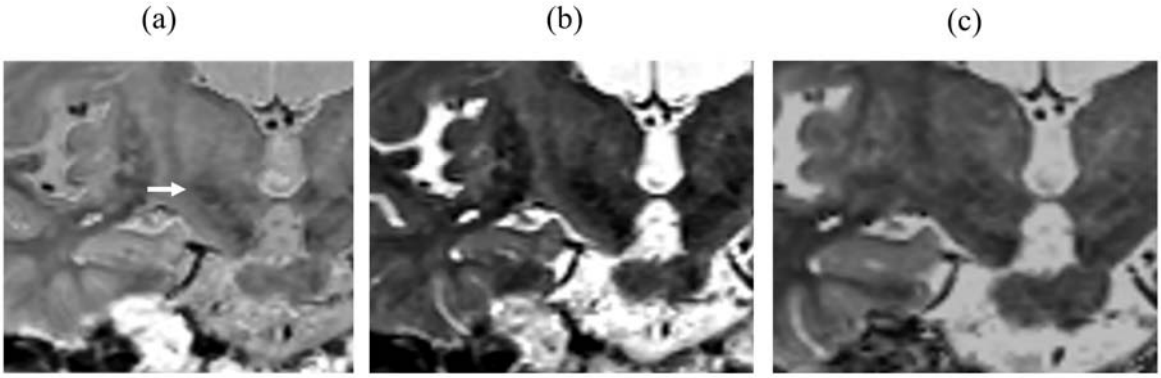

FIGURE 3

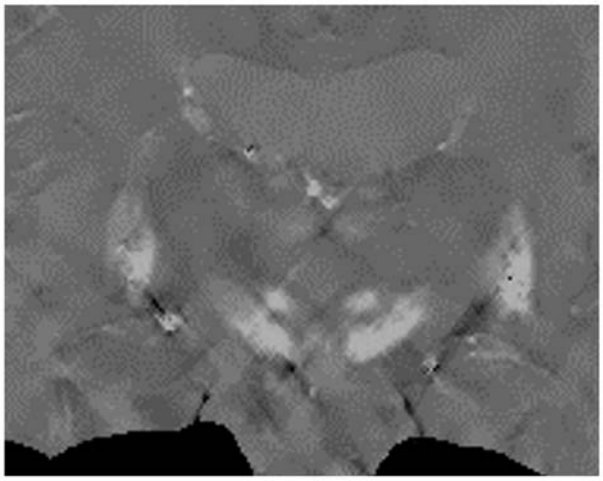

Table 1. The demographic and clinical data of the subjects

	healthy volunteers (n=5)	PD patients		
	with SyMRI and QSM	with SyMRI (n=7)	with QSM (n=15)	*p*
Sex: (M/F)	(5/0)	(3/4)	(6/9)	1
Age (years): median (IQR)	28 (28-29)	70 (69-79)	72 (68-79)	0.805
Onset (years), median (IQR)		67 (67-67)	68 (65.5-75)	1
Disease duration (months), median (IQR)		32.0 (18.0-36.0)	66.7 (27.55-86.15)	0.116
H & Y stage, median (range)		3 (1-4)	3 (2-3)	0.536

Note. M, male; F, female; IQR, interquartile range; H & Y stage, Hoehn and Yahr stage; PD, Parkinson's disease; SyMRI, synthetic MRI; QSM, quantitative susceptibility mapping.

Table 2. Sequence parameters of coronal regular SyMRI and optimized SyMRI

	regular SyMRI		optimized SyMRI	
	T2WI	STIR	healthy volunteers	PD patients
TR (ms)	4000	15000	5000	4387-11833*
TE (ms)	100	5	40	18-76*
TI (ms)		300		0-5936*
ETL	5	5	5	5
BW (kHz)	150	150	150	150
FOV (cm)	240	240	240	240
ST (mm)	2.2	2.2	2.2	2.2
F-resol	0.75	0.75	0.75	0.75
P-resol	0.94	0.94	0.94	0.94
NEX	1	1	1	1
AF	2	2	2	2
AT (minute: second)	12:14	12:14	12:14	12:14

Note. TR, repetition time; TE, echo time; TI, inversion time; ETL, echo train length; BW, band width; FOV, field of view; ST, slice-thickness; F- resol, frequency resolution; P-resol, phase resolution; NEX, number of excitation; AF, acceleration factor; AT, acquisition time; SyMRI, synthetic MRI; PD, Parkinson's disease.

* range

Table 3. STN scores

	healthy volunteers (n=5)				PD patients			
	regular SyMRI		optimized SyMRI	QSM	regular SyMRI (n=7)		optimized SyMRI (n=7)	QSM (n=15)
	T2WI	STIR			T2WI	STIR		
Radiologist 1: median (IQR)	2.5 (2-3)*	0 (0-0)	3 (3-3)*	3 (3-3)*	0.5 (0-1.75)	0 (0-0)	3 (3-3)**	3 (2-3)**
Radiologist 2: median (IQR)	3 (3-3)*	0 (0-0)	3 (3-3)*	3 (3-3)*	1 (0-1)*	0 (0-0)	3 (2.25-3)**	3 (3-3)**
Interobserver agreement	0.5714	NA	NA	NA	0.8931	0.6316	0.4324	0.5181

Note. STN, subthalamic nucleus; PD, Parkinson's disease; SyMRI, synthetic MRI; QSM, quantitative susceptibility mapping; IQR, interquartile range; NA, not applicable.

*P<0.05, Significantly higher in comparison to Sy-STIR.

**P<0.05, Significantly higher in comparison to regular SyMRI (T2WI and STIR)

Table 4. Measurements of the contrast-to-noise ratio (CNR)

		healthy volunteers (n=5)				PD patients			
		regular SyMRI		optimized SyMRI	QSM	regular SyMRI (n=7)		optimized SyMRI (n=7)	QSM (n=15)
		T2WI	STIR			T2WI	STIR		
STN-ZI	Median	6.7*	0.8	7.8*	19.1***	3.3*	1	3.2*	16.8***
	Interquartile range	5.0-9.0	0.2-1.2	5.7-9.1	14.2-27.2	2.1-4.3	0.8-1.9	3.0-4.3	14.0-21.7
	Range	3.4-13.2	0-3.0	3.1-11.1	11.6-47.1	1.2-7.6	0.2-3.0	2.0-6.0	5.5-32.8
STN-SN	Median	3.1	4.6	6.6	10.1	1.4	1	2.2	5.7***
	Interquartile range	2.2-3.8	4.0-5.6	5.9-7.2	4.0-26.9	0.6-2.4	0.2-2.4	1.5-3.1	2.5-11.2
	Range	0.3-4.8	0.5-7.5	0.6-9.7	1.1-29.3	0-5.1	0-4.4	0.7-6.9	0.7-16.2

Note. STN, subthalamic nucleus; ZI, zona incerta; SN, substantia nigra; PD, Parkinson's disease; SyMRI, synthetic MRI; QSM, quantitative susceptibility mapping.

*P<0.05, Significantly higher in comparison to Sy-STIR

**P<0.05, Significantly higher in comparison to regular SyMRI (T2WI and STIR)

***P<0.05, Significantly higher in comparison to optimized SyMRI and SyMRI (T2WI and STIR)

Figure legends

Figure. 1: Examples of region of interest delineation in a healthy 28-year-old male volunteer.

(a) Coronal optimized SyMRI shows the STN (1), its superior neighbor, presumably the ZI (2), the border (3) between the STN and the SN (4), and the thalamus (4).

(b) A coronal QSM image shows the STN (1), its superior neighbor, presumably the ZI (2), the border (3) between the STN and the SN (4), and the thalamus (4).

For the visualization score of the STN, the coronal optimized SyMRI and QSM images are rated as Score 3; the STN was well defined and clearly differentiable from its superior neighbor, presumably the zona incerta, and its inferior neighbor, the SN.

Figure. 2: The STN score in a 68-year-old female with PD.

(a) Coronal optimized SyMRI, (b) Sy-T2WI, and (c) Sy-STIR.

On the coronal optimized SyMRI image, the right STN appears hypointense and lenticular (arrow). The STN is clearly differentiated from the surrounding brain tissue on coronal optimized SyMRI (Score 3), but not on Sy-T2WI (Score 2) or Sy-STIR (Score 0).

Figure. 3: The STN score in an 84-year-old female PD patient.

A QSM image from the PD patient is rated as Score 2; only the superior border of the STN is visible. There is no visible border between the STN and SN.